

Investigating the NCQ scaling of elliptic flow at LHC with a multiphase transport model

Liang Zheng^{1,2a}, Hui Li¹, Hong Qin², Qi-Ye Shou^{1b}, and Zhong-Bao Yin^{1c}

¹ Key Laboratory of Quark and Lepton Physics (MOE) and Institute of Particle Physics, Central China Normal University, Wuhan 430079, China,

² School of Mathematics and Statistics, Central China Normal University, Wuhan, 430079, China

Abstract. The number of constituent quark (NCQ) scaling behavior of elliptic flow has been systematically studied at the LHC energy within the framework of a multiphase transport model (AMPT) in this work. With the variation of the fragmentation parameters, collision centrality and system energy, we find that the initial conditions of parton dynamics are more important than the final state parton cascade process for the existence of NCQ scaling when the hadronic interaction is off in Pb-Pb collisions. By turning on the hadron interaction process, the impacts of hadronic evolution are found to be responsible for a significant violation to the well established scaling structure. Our study suggests the interpretation of NCQ scaling is not only subject to the hadronization mechanism but also to the initial conditions of parton evolution as well as the hadronic interactions especially for the LHC experiments.

PACS. 25.75.Ld Collective flow – 24.10.Lx Monte Carlo simulations (including hadron and parton cascades and string breaking models) – 21.65.Qr Quark matter

1 Introduction

The formation and the evolution of the color-deconfined strongly interacting matter, quark-gluon plasma (QGP) [1], have been studied via relativistic heavy-ion collisions for decades. As one of the most important quantities, elliptic flow (v_2), which is defined as the second-order Fourier component of the particle azimuthal distribution [2], receives considerable attention and plays an essential role in studying the collective motion and bulk property of the QGP. The transverse momentum (p_T) dependence of v_2 serves as a unique probe to test different physics processes. At low p_T , v_2 is commonly used to extract the information of the early stage of the collisions, such as the pressure gradients, the degree of thermalization, and the equation of state, *etc* [3, 1, 4]. In addition, for a given low p_T value, v_2 of different particles are observed to be ordered by mass with heavier particles having the smaller v_2 and vice versa.

In the intermediate p_T region, v_2 is considered to be able to reveal the production mechanism of hadron. Results from RHIC show the p_T differential v_2 of particles tend to group based on their hadron types, baryons or mesons [5, 6, 7]. This phenomenon has been interpreted as

a signature of quark recombination or coalescence models, in which hadrons are formed from the combination of the neighboring constituent quarks in phase space [8, 9, 10]. More intriguingly, it is also proposed by such models that v_2 of different hadrons, when scaled by the number of constituent quarks (NCQ or n_q), could approximately exhibit a uniform behavior with v_2/n_q vs. p_T/n_q falling on a universal curve, namely,

$$\frac{v_2^B(p_T/3)}{3} = \frac{v_2^M(p_T/2)}{2}, \quad (1)$$

where superscript B (M) denotes baryons (mesons) consisting of 3(2) constituent quarks.

This feature has been observed at RHIC with surprising accuracy [11, 12, 13, 14, 15], and furthermore, it can also manifest itself when investigating the transverse kinetic energy ($m_T - m_0$) dependence of v_2 [11, 16]. Such a scaling can be understood as a consequence of the coalescence mechanism and the deduction of v_2 in the partonic evolution stage. For a narrow hadronic wave function in momentum space, the v_2 of a given type of meson with valence quark a and b reads [17],

$$v_2^M(p_T) = v_2^a(x_a p_T) + v_2^b(x_b p_T), \quad (2)$$

where x_a and x_b are fixed momentum fractions with $x_a + x_b = 1$. In the case of a and b having the same v_2 , Eq. (2)

^a zhengl@mails.cnu.edu.cn

^b qiye.shou@cern.ch

^c zbyin@mail.cnu.edu.cn

can be simplified to

$$v_2^h(p_T^h) = n_q v_2^q(p_T^h/n_q), \quad (3)$$

where superscript h (q) represents hadrons (quarks) and $n_q = 3$ (2) for baryons (mesons). This treatment has also been extended to higher-order flow harmonics [18, 19].

For many years, it is widely believed that the NCQ scaling is a natural result and an important evidence of the dominance of quark degrees of freedom in the evolution of QGP. Recently, however, both PHENIX [20] and ALICE experiments [21] have reported the deviation of the scaling properties in heavy-ion collisions, and the latter, in particular, announced the violation at the level of $\pm 20\%$ for all centrality intervals, which triggers various theoretical concerns and reconsiderations [22, 23, 24]. In Ref. [25], the authors argue that the high phase-space density of constituent quarks should be the key reason of the broken of NCQ scaling. Nevertheless, the formation of the scaling properties is the consequence of a succession of interaction processes at both partonic-level and hadronic-level. Therefore, it is worthwhile to study the integrated effect instead of a single factor through a transport model to understand the contribution from each intermediate process.

In this work we perform a systematic study of the possible factors contributing to the deviation of the v_2 NCQ scaling at the LHC energy with the string-melting version of the AMPT model, in which the parton coalescence mechanism and hadron cascade process are jointly provided. This paper is organized as follows. In Sec. 2 and Sec. 3, we give a brief introduction to the AMPT model and the methodology to calculate the azimuthal flow in our study. The results of identified particle flow confronted with NCQ scaling is presented in Sec. 4.1. To have a systematic understanding to the collective anisotropy at the LHC, we also study the centrality dependence of the constituent quark number scaled flow behavior in Sec. 4.2. We further explore the hadronic evolution effects including resonance decay and hadron rescattering for different particles in Sec. 4.3. The energy dependence of the NCQ scaling has been studied by investigating identified flow at $\sqrt{s_{NN}} = 5.02$ TeV in Sec. 4.4.

2 AMPT model

The AMPT model [26] is a hybrid transport model widely used in the description of collective behavior in heavy ion collisions. It uses initial parton conditions generated in HIJING [27]. The parameters a and b used in HIJING determine the Lund string fragmentation function as $f(z) \propto z^{-1}(1-z)^a \exp(-bm_{\perp}^2/z)$, where z is the light-cone momentum fraction of the produced hadron of transverse mass m_{\perp} with respect to the fragmenting string.

In the string melting version of AMPT model, initial strings from HIJING are converted to their valence quarks and antiquarks. The evolution of the partonic phase is implemented with the Zhang's Parton Cascade (ZPC) model [28] which calculates the parton-parton scattering using cross sections $\sigma \approx \frac{9\pi\alpha_s^2}{2\mu^2}$ based on a Debye screening mass μ .

After the partons stop interaction in ZPC, a hadronization process based on the quark coalescence model has been applied to the quarks, which combines the nearest quarks in coordinate space into hadrons. Hadronic stage evolution is then performed to the hadrons formed during quark coalescence, handled by the ART model with the input cross section for different hadron-hadron scattering channels. The hadronic interactions in this step will be terminated at a cutoff time $t_{max} = 30$ fm/c by default, when all the observables of interest are stable at final state.

In this work we use the program version with string melting Ampt-v1.26t5-v2.26t5. It is proposed that in this version of AMPT model the set of Lund string fragmentation parameters $a = 0.3$, $b = 0.15$ GeV $^{-2}$, (set A) along with $\sigma = 3$ mb and $\mu = 2.3$ fm $^{-1}$ can be used to describe the rapidity density, transverse momentum spectrum and elliptic flow at the LHC energy simultaneously [29]. Compared to other widely used parameter sets, a small b is applied to generate large mean transverse momentum of the initial hadrons in this tuning. As the effective string tension $\kappa \propto 1/[b(2+a)]$ is quite large due to the selection of b value, an upper limit of PARJ(2) on the relative production of strange to nonstrange quarks is set to 0.4 to constrain the strangeness production. We will stick to this parameter set in the following study, unless otherwise specified.

3 Event Plane Method

In this study, we will use the event plane method as illustrated in [30] to calculate the elliptic flow in AMPT. The procedures of this method will be briefly described here. The momentum distribution of emitted particles can be expressed as follows:

$$E \frac{d^3N}{d^3p} = \frac{1}{2\pi} \frac{d^2N}{p_T dp_T dy} (1 + \sum_n 2v_n \cos[n(\phi - \Psi_n)]), \quad (4)$$

where ϕ is the azimuthal angle of the particle in transverse plane, y and p_T represent the rapidity and transverse momentum, v_n is the n -th harmonic flow. The event plane angle Ψ_n is determined with the momentum of all the particles within $|\eta| < 0.8$:

$$\Psi_n = \frac{1}{n} \left[\arctan \frac{\sum_i p_T^i \sin(n\phi_i)}{\sum_i p_T^i \cos(n\phi_i)} \right], \quad (5)$$

where the subscript i runs over all the selected particles in that event. The selected particle of interest has been excluded when building up the corresponding event plane to avoid the auto-correlation. The azimuthal flow with respect to this event plane is:

$$v_n(p_T) = \langle \cos[n(\phi - \Psi_n)] \rangle. \quad (6)$$

The bracket $\langle \dots \rangle$ denotes an average over all particles in the event sample with transverse momentum p_T . Since the reconstructed event plane is only an approximation to the true reaction plane, the observed azimuthal flow coefficient

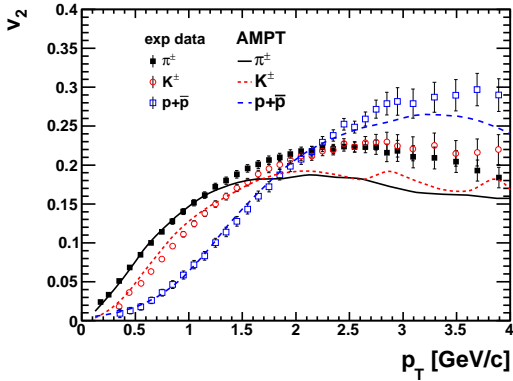


Fig. 1. Differential v_2 on p_T of π K and p in mid-rapidity for Pb-Pb collisions at $\sqrt{s_{NN}} = 2.76$ TeV for centrality 30-40% with input parameters $a = 0.3$, $b = 0.15$ GeV^{-2} , $\sigma = 3$ mb and $\mu = 2.3$ fm^{-1} . Data is from the ALICE experiment [21].

obtained in Eq. 6 has to be corrected by the event plane resolution. In this work, we restrict ourselves to the elliptic flow of particles within pseudorapidity window $|\eta| < 0.8$ for Pb-Pb collisions at the LHC energy. Meanwhile, due to the large multiplicity generated at the LHC energy scale, the resolution of Ψ_n can be practically taken to be 100% for central and semi-central collisions.

The comparison of the AMPT model simulation results with parameters listed in the last section and the measured experimental data from ALICE [21] is shown in Fig. 1 for the identified particle elliptic flow at Pb-Pb $\sqrt{s_{NN}} = 2.76$ TeV with centrality 30-40%. It is observed that the AMPT model generated v_2 agrees very well with the ALICE data to a large extent.

4 Results and Discussions

4.1 Identified particle elliptic flow at Pb-Pb $\sqrt{s_{NN}} = 2.76$ TeV without hadronic evolution

The anisotropy in AMPT is developed initially through parton level evolution. The hadron level flow is derived from the partonic anisotropy through a quark coalescence model and then modified in the hadronic evolutions. We exclude the hadron phase contribution by focusing on the primordial particles generated directly after coalescence procedure at this moment, and leave the discussion of hadronic evolution effect to the later part in Sec. 4.3. In the following text, we refer to the particles formed right after coalescence as the primordial particles.

Another parameter set tuned to be applicable both at RHIC and LHC energy scale with $a = 0.5$, $b = 0.9$ GeV^{-2} , (set B) $\sigma = 1.5$ mb and $\mu = 3.2$ fm^{-1} [31,32] has also been used in a wide range of phenomenological studies. The set B parameters, corresponding to a smaller string tension $\kappa_B \approx 1/6\kappa_A$, are found to reasonably reproduce the azimuthal flow but underestimates the particle yield for large p_T at the LHC. To provide a systematic understanding on the behavior of the identified particle elliptic

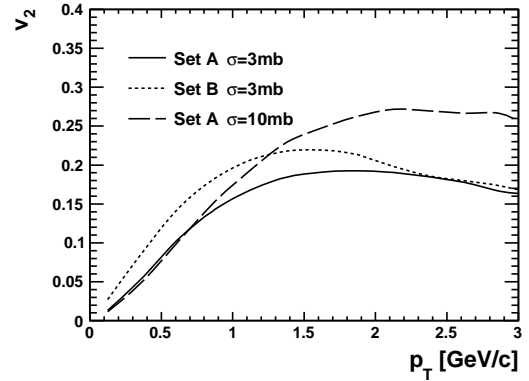


Fig. 2. Differential v_2 on p_T of mid-rapidity charged pion in Pb-Pb collisions at $\sqrt{s_{NN}} = 2.76$ TeV for centrality 30-40% with different input parameters. The particles are formed right after coalescence procedure.

flow formed in AMPT, we will compare the effects of set A and set B (details can be found in Tab. 1) with the same parton-parton cross section $\sigma = 3$ mb. Meanwhile, a variation on the parton scattering cross section $\sigma = 10$ mb based on set A has also been provided. The simulation has been performed for Pb-Pb collisions at $\sqrt{s_{NN}} = 2.76$ TeV with the centrality of 30-40%.

Table 1. Details of set A and set B parameters

	a	b (GeV^{-2})
set A	0.3	0.15
set B	0.5	0.9

We show in Fig. 2 the comparison of different input parameters on the primordial charged pion v_2 as a function of p_T . It can be found in this comparison that larger parton-parton cross section leads to a much stronger v_2 in high p_T region, while the low p_T region v_2 is only slightly suppressed. On the other hand, for the fixed $\sigma = 3$ mb, input parameters with set B generate significantly larger v_2 in the low p_T region, while both the two sets reach a similar v_2 for large p_T . We also make a comparison for the selected hadron v_2 in Fig. 3 based on different string tensions. Although the overall flow is enhanced with set B parameters, the particle v_2 still exhibits the mass ordering feature at low p_T for both set A and set B. It is pointed out in earlier studies that this ordering effect is mainly from kinematics in the quark coalescence process and later hadronic rescatterings [33]. Thus, one would naturally expect it is independent of the initial state conditions.

At the intermediate p_T region, the meson and baryon flow are supposed to be amplified two/three-fold compared to that of the constituent quarks, leading to the number of constituent quark scaling behavior. This behavior can be well explained in the quark coalescence mechanism, when the constituent quarks coalesce into a meson or baryon in a collimated way. We investigated the v_2 NCQ scaling behavior of some selected hadrons shown in Fig. 4 based on

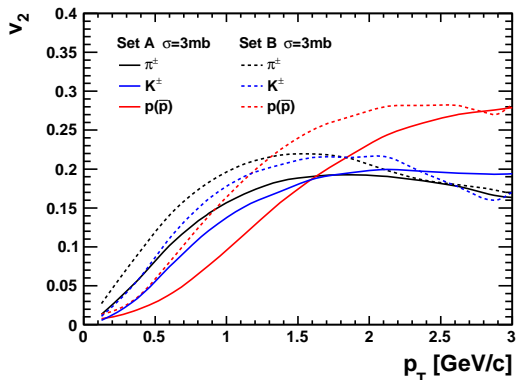


Fig. 3. (Color online) Differential v_2 on p_T for selected particles at mid-rapidity with different input parameters in Pb-Pb collisions at $\sqrt{s_{NN}} = 2.76$ TeV for centrality 30-40% based on fixed parton rescattering cross section $\sigma = 3$ mb. The particles are formed right after coalescence procedure.

a variety of input parameter sets for the Pb-Pb collisions at $\sqrt{s_{NN}} = 2.76$ TeV in centrality 30-40%. It is found that the NCQ scaling phenomena relies on the choice of the input parameters used to produce the initial partons. The scaling behavior is evidently violated with the set B input parameters while it still holds to a large extent using the parameters of set A. By changing the parton-parton interaction cross section from $\sigma = 3$ mb to $\sigma = 10$ mb, one can see the v_2 with set A parameters still exhibits the NCQ scaling within the intermediate p_T range of $0.3 < (m_T - m_0)/n_q < 1$ GeV.

To quantify the size of the violation to NCQ scaling, we defined the following quantity

$$\chi = \sqrt{\Sigma_{\pi,K} \left(\frac{v_2^{\pi,K}/n_q^{\pi,K} - v_2^p/n_q^p}{v_2^p/n_q^p} \right)^2}, \quad (7)$$

where the v_2 are obtained for the integrated flow in the range $0.3 < (m_T - m_0)/n_q < 1$ GeV. Larger χ indicates stronger violations. It is found that the magnitude of the violation to the NCQ scaling shown in 30-40% set A and 30-40% set B can be quantified by χ as: 0.06, 0.14, respectively. Smaller χ exists in the set A parameter results is consistent with our expectations.

As it is known that the change of fragmentation parameter set will modify the initial quark momentum and multiplicity distribution from string melting, we explored the parton number distribution dependent on the transverse momentum at the time of coalescing to final state hadrons in Fig. 5. It is observed in this plot the partons from initial conditions generated with set B parameter are much softer than that with set A. With the same initial geometry configuration, the partons generated with set B stay in the overlap region effectively longer and leading to a higher parton-parton interaction rate, which breaks the initial scaling pattern. On the other hand, the change in parton rescattering cross section from $\sigma = 3$ mb to 10 mb is not casting much impact on the freeze out parton momentum distribution especially in the p_T range relevant

for NCQ scaling. Thus, one may not see any variation to the NCQ scaling from parton rescattering.

It can be understood in this comparison that the scaling behavior is related to the relative size of identified particle v_2 , thus decoupled from the global v_2 strength governed by the parton-parton interaction cross section. On the other hand, the initial parton conditions generated by different fragmentation parameters a, b may play an important role in determining the collimation of constituent quarks during the coalescence of hadrons, which in the end modifies the v_2 NCQ scaling behavior. In the following studies, we will rely on the input parameters of set A along with $\sigma = 3$ mb to systematically explore the stability of v_2 NCQ scaling.

4.2 Centrality dependence of NCQ scaling

One can observe the NCQ scaling with the input parameters of set A in AMPT model for Pb-Pb semi-central collisions at the LHC energy, it will be interesting to investigate the robustness of this scaling behavior with different collision centralities. For this purpose, we will study the centrality dependence of the NCQ scaling in Pb-Pb collisions at $\sqrt{s_{NN}} = 2.76$ TeV.

Fig. 6 shows the NCQ scaling behavior of some selected hadrons within $|\eta| < 0.8$ for the centrality of 0-1% (impact parameter b : 0-1.58 fm), 39-40% (b : 9.86-9.99 fm) and 49-50% (b : 11.05-11.17 fm). The centrality window has been fixed to a narrow range to remove the centrality variation effects. One can observe in the most central bin 0-1%, the n_q scaled v_2 for proton is systematically smaller than that for pion and kaon, while in peripheral collisions the NCQ scaling is well preserved. We have performed a χ calculation with the published ALICE data [21] and find similar conclusion that $\chi = 0.29$ for centrality 0-5% and $\chi = 0.17$ for centrality 30-40%.

We integrated the p_T differential flow over the corresponding range in $0.3 < (m_T - m_0)/n_q < 1$ GeV in several centrality bins between 0-70% with the result shown in Fig. 7. The integrated flow for all three particle species rises from central to semi-central collisions and then drops after reaching the maximum in semi-central collisions.

There is also a trend shown in Fig. 8 that the n_q scaled integrated v_2 between proton and pion grows monotonously from central to peripheral collisions, approaching unity which satisfies the NCQ scaling within the centrality range 30-60%. On the other hand, the ratio between K and π is flatly distributed around unity for all centralities.

To sum up, we observe that the NCQ scaling of v_2 is violated in Pb-Pb central collisions, while it is recovered during the transition to the peripheral collisions.

4.3 Impact of hadronic interactions for identified particle elliptic flow

One postulation for the violation to the flow NCQ scaling at LHC energy is the distortion of v_2 developed at partonic stage by later hadronic interactions. We explored the

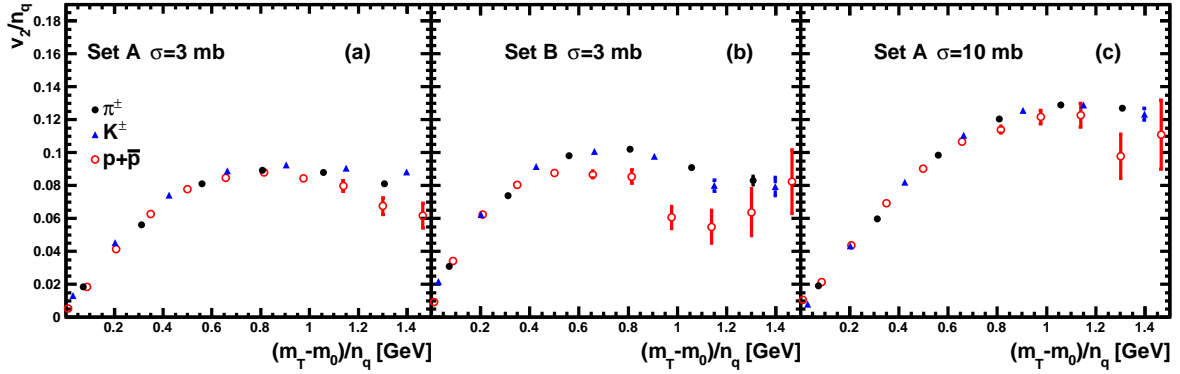


Fig. 4. (Color online) Number of constituent quark scaled v_2 for selected hadrons right after coalescence procedure with parameters Set A $\sigma = 3$ mb, Set B $\sigma = 3$ mb, and Set A $\sigma = 10$ mb for Pb-Pb collisions at $\sqrt{s_{NN}}=2.76$ TeV with the centrality 30-40%. Charged pion, kaon and proton results are labeled by the solid dots, triangles and open circles, respectively.

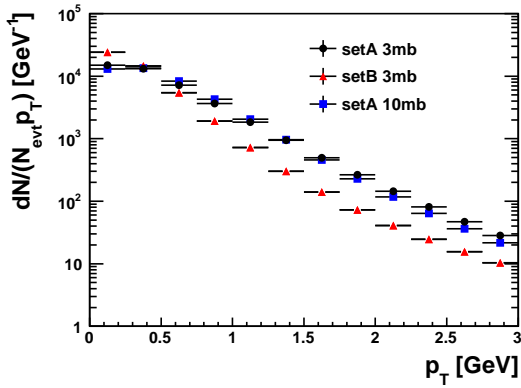


Fig. 5. p_T distribution of partons at freeze out in Pb-Pb collisions at $\sqrt{s_{NN}} = 2.76$ TeV for centrality 30-40% with different input parameters and parton rescattering cross sections.

impacts of possible different hadronic interactions (including resonance decay and hadron rescattering in hadronic evolution stage) on the v_2 of some selected hadrons. We switched on the contribution from resonance decay and hadronic rescattering independently and compared the impacts of these hadronic effects with respect to the flow developed for the primordial particles mainly from quark evolution phase. The hadron rescattering strength is mediated by maximum allowed hadronic rescattering time t_{max} in AMPT.

It is shown in Fig. 9 that the comparison of the p_T differential v_2 with different hadronic effects divided by that for the primordial particles formed right after coalescence. These comparisons use the default hadronic rescattering time $t_{max} = 30$ fm/c. Hadronic rescattering seems to destruct the azimuthal anisotropy formed during the quark stage at low p_T for protons and kaons, while resonance decay enlarges low p_T v_2 and reduces high p_T v_2 for these two particle species. On the other hand, the pion v_2 is following the opposite trend. A kink like behavior is observed for pion hadron rescattering dominated flow

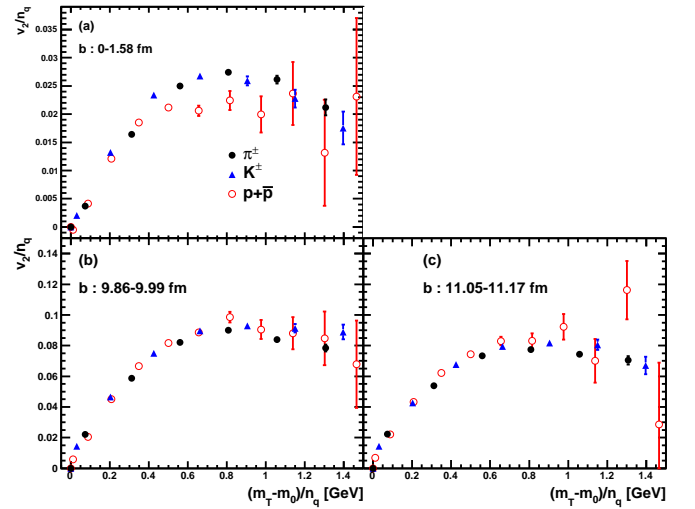


Fig. 6. (Color online) Number of constituent quark scaled v_2 for selected hadrons right after coalescence procedure with parameters Set A and $\sigma = 3$ mb for the centrality 0-1% (b: 0-1.58 fm), 39-40% (b: 9.86-9.99 fm) and 49-50% (b: 11.05-11.17 fm) in Pb-Pb collisions at $\sqrt{s_{NN}}=2.76$ TeV. Charged pion, kaon and proton results are labeled by the solid dots, triangles and open circles, respectively.

ratio. If we put on the resonance decay along with hadron rescattering step by step, a suppression is observed for the intermediate p_T flow of all three particles and for proton this effect is much stronger. Indicated by this comparison, the distortion of elliptic flow from hadronic evolution is an important source for the violation of NCQ scaling.

We studied the hadron interaction strength dependence of the identified particle flow integrated over $0.3 < (m_T - m_0)/n_q < 1$ GeV in Fig. 10 by varying t_{max} parameter in AMPT. Larger t_{max} suggests stronger hadronic interaction contributions. The notation $t_{max} = -10$ fm/c denotes the flow of primordial particles formed right after coalescence. v_2 with $t_{max} = 0.3$ fm/c effectively turns off the hadron rescattering but includes the resonance decay. As

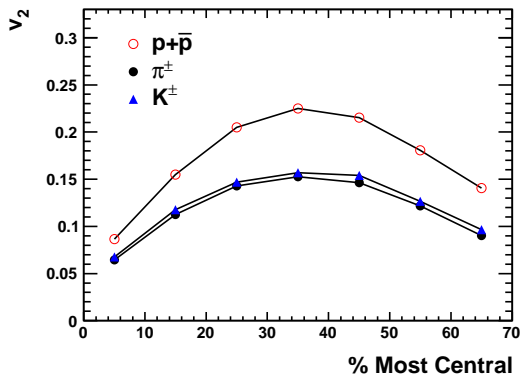


Fig. 7. (Color online) Integrated flow within $0.3 < (m_T - m_0)/n_q < 1$ GeV for pion, kaon and proton varying with the centrality.

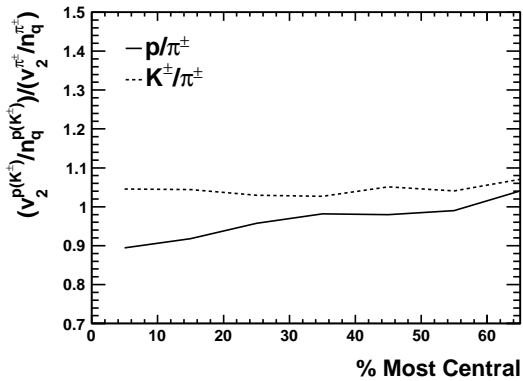


Fig. 8. Ratio of integrated flow within $0.3 < (m_T - m_0)/n_q < 1$ GeV for proton over pion and kaon over pion varying with the centrality.

can be seen, resonance decay destroys the collectivity for all three particles in the intermediate p_T range, comparing $t_{max} = -10$ fm/c to $t_{max} = 0.3$ fm/c. The integrated v_2 decreases with t_{max} in general, although the dependence is very weak when t_{max} is greater than 15 fm/c. The difference between proton over pion v_2 ratio and unity becomes enlarged with rising t_{max} suggests that larger violation to NCQ scaling is generated due to stronger hadronic interactions.

In order to understand the dependence of the hadron evolution impact on the violation to NCQ scaling, we listed the values of χ calculated at different time scales in Tab. 2 based on Eq. 7. It is observed that the magnitude of violation to NCQ scaling before hadronic interaction stage is relatively small as low as 0.06. In case the resonance decay is included, the violation degree rapidly grows to 0.16. The impact of hadron rescattering is dependent on the allowed maximum time length of hadron evolution.

Table 2. χ at different time scale

	primordial	w/ decay	$t_{max}=15$ fm/c	$t_{max}=90$ fm/c
χ	0.06	0.16	0.19	0.24

4.4 v_2 NCQ scaling at $\sqrt{s_{NN}}=5.02$ TeV

The particle yield and azimuthal anisotropy size are found to slightly increase with the collision energy from $\sqrt{s_{NN}} = 2.76$ TeV to $\sqrt{s_{NN}} = 5.02$ TeV. It is then expected to see little variation on the NCQ scaling behavior of the identified particle elliptic flow with the top Pb-Pb collision energy at the LHC. We will explore the v_2 NCQ scaling within AMPT model at $\sqrt{s_{NN}}=5.02$ TeV based on the input parameter set A with $\sigma = 3$ mb. These parameters have been extensively used in the predictions on various observables in Pb-Pb collisions at $\sqrt{s_{NN}}=5.02$ TeV [34].

It can be found in Fig. 11 that the n_q scaling works to a large extent before hadronic evolution takes place in the semi-central collisions with centrality 30-40%. The centrality dependence and hadronic interaction impact are similar to what has been uncovered in the studies for $\sqrt{s_{NN}}=2.76$ TeV in this work. Hadronic interactions are also important to account for the violation of NCQ scaling at this energy scale.

5 Summary

In this work, we have systematically investigated the NCQ scaling of elliptic flow at the LHC energy using the AMPT model. We find the NCQ scaling exists with the initial conditions generated in the semi-central collisions based on the Lund string parameter set carrying larger string tension if the hadronic interaction is off. The larger number of initial partons from the conditions generated with fragmentation parameter carrying smaller string tension or in central collisions could lead to more scatterings and violate NCQ scaling in the current AMPT framework. It is shown in these comparisons that the NCQ scaling structure not only depends on the hadronization procedure but also relies on the parton dynamics at the initial stage before evolution.

The impact of the hadronic interaction on the v_2 of selected hadrons has been studied in details. Resonance decay and hadron rescattering modify the v_2 magnitude differently for different particle species. A sizable distortion to the NCQ scaling arises due to the effects introduced by the hadronic interactions. Our quantitative analysis shows the contribution from resonance decay and hadron rescattering are both important in the development of the violation to NCQ scaling.

Besides, it must be aware that the parton coalescence mechanism in the current AMPT model is performed in the coordinate space of constituent quarks. There is a chance that the momentum collimation is not well preserved during the coalescence procedure, which might lead to a violation to the exact NCQ scaling. It can be of great interest to test the scaling behavior from a coalescence

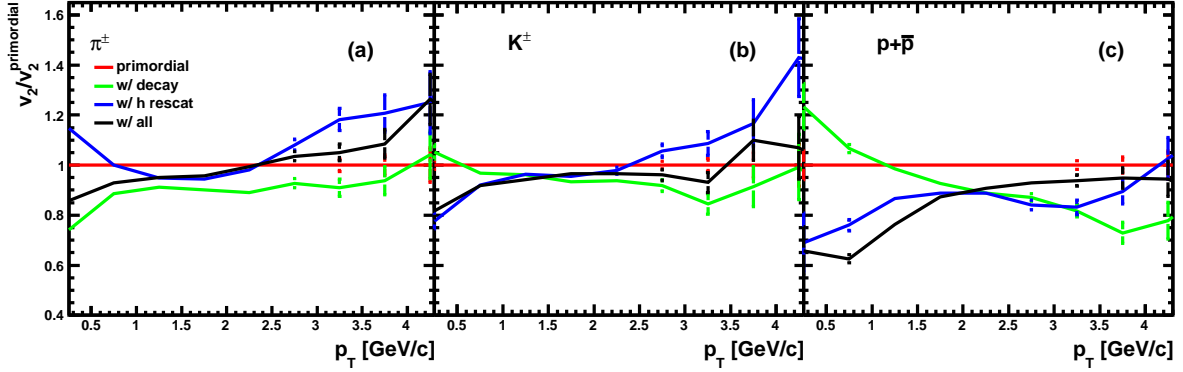


Fig. 9. (Color online) Ratio of v_2 with different hadronic effects divided by that right after coalescence for pions (a), kaons (b) and protons (c). The elliptic flow is calculated for Pb-Pb collisions at $\sqrt{s_{NN}} = 2.76$ TeV with the centrality of 30-40% using parameters set A and $\sigma = 3$ mb. $t_{max} = 30$ fm/c for the allowed hadron evolution time.

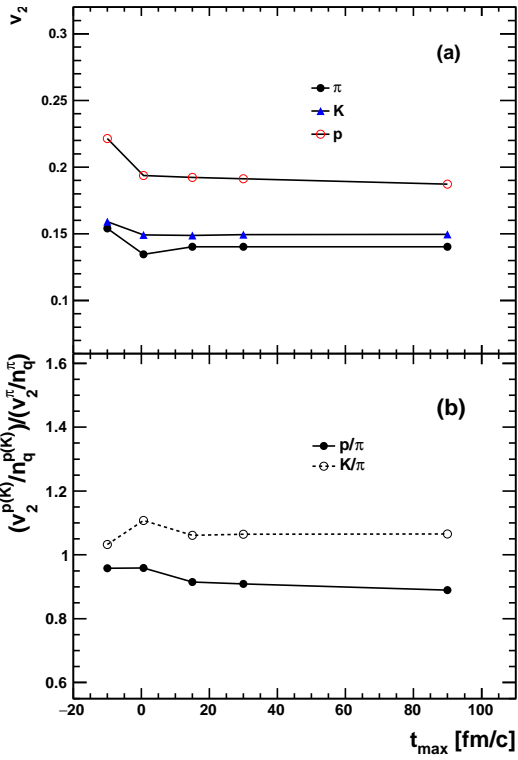


Fig. 10. (Color online) Integrated flow for selected particles within $0.3 < (m_T - m_0)/n_q < 1$ GeV for pion, kaon and proton (a) along with the integrated flow ratio of proton over pion and kaon over pion (b) varying with t_{max} . The elliptic flow is calculated for Pb-Pb collisions at $\sqrt{s_{NN}} = 2.76$ TeV with the centrality of 30-40% using parameters set A and $\sigma = 3$ mb.

procedure implemented with collimated quarks in both momentum and coordinate space in the future.

We thank Zi-Wei Lin, Guo-Liang Ma and Jun Xu for helpful discussions. This work was supported by NSFC (11475068 and 11605070), China Postdoctoral Science Foundation (2016M590703),

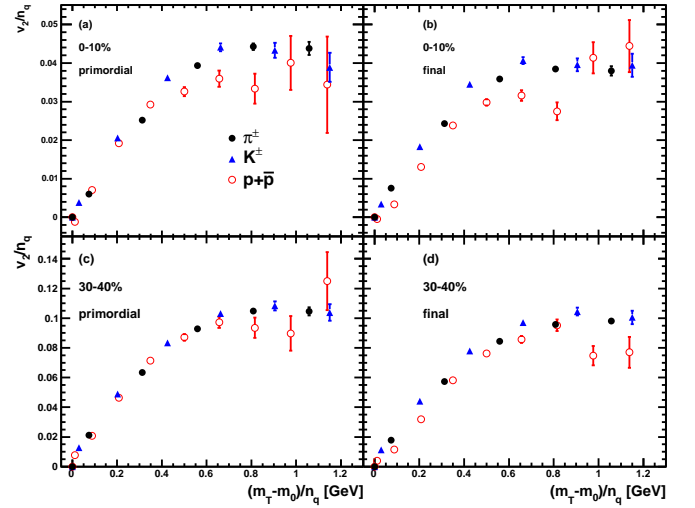


Fig. 11. (Color online) v_2 NCQ scaling at $\sqrt{s_{NN}} = 5.02$ TeV with the centrality 0-10% and 30-40% using parameters set A, $\sigma = 3$ mb before (Left column) and after (Right column) hadronic interactions.

the National Key Research and Development Program of China under Grant No.2016YFE0100900. LZ acknowledges support by the programme of Introducing Talents of Discipline to Universities (B08033).

References

1. M. Gyulassy, L. McLerran, Nucl. Phys. **A750**, 30 (2005), nucl-th/0405013
2. P.F. Kolb, U.W. Heinz (2003), nucl-th/0305084
3. C. Shen, U. Heinz, P. Huovinen, H. Song, Phys. Rev. **C84**, 044903 (2011), 1105.3226
4. L. Adamczyk et al. (STAR), Phys. Rev. **C88**, 014902 (2013), 1301.2348
5. B.I. Abelev et al. (STAR), Phys. Rev. **C75**, 054906 (2007), nucl-ex/0701010

6. S.S. Adler et al. (PHENIX), Phys. Rev. Lett. **91**, 182301 (2003), [nucl-ex/0305013](#)
7. J. Adams et al. (STAR), Phys. Rev. **C72**, 014904 (2005), [nucl-ex/0409033](#)
8. D. Molnar, S.A. Voloshin, Phys. Rev. Lett. **91**, 092301 (2003), [nucl-th/0302014](#)
9. J. Jia, C. Zhang, Phys. Rev. **C75**, 031901 (2007), [hep-ph/0608187](#)
10. L.X. Han, G.L. Ma, Y.G. Ma, X.Z. Cai, J.H. Chen, S. Zhang, C. Zhong, Phys. Rev. **C84**, 064907 (2011), [1105.5415](#)
11. S. Afanasiev et al. (PHENIX), Phys. Rev. Lett. **99**, 052301 (2007), [nucl-ex/0703024](#)
12. J. Adams et al. (STAR), Phys. Rev. Lett. **92**, 052302 (2004), [nucl-ex/0306007](#)
13. A. Adare et al. (PHENIX), Phys. Rev. Lett. **98**, 162301 (2007), [nucl-ex/0608033](#)
14. L. Adamczyk et al. (STAR), Phys. Rev. **C93**(1), 014907 (2016), [1509.08397](#)
15. B.I. Abelev et al. (STAR), Phys. Rev. **C77**, 054901 (2008), [0801.3466](#)
16. Z. Tang, L. Yi, L. Ruan, M. Shao, H. Chen, C. Li, B. Mohanty, P. Sorensen, A. Tang, Z. Xu, Chin. Phys. Lett. **30**, 031201 (2013), [1101.1912](#)
17. R.J. Fries, V. Greco, P. Sorensen, Ann. Rev. Nucl. Part. Sci. **58**, 177 (2008), [0807.4939](#)
18. X. Sun (STAR), J. Phys. Conf. Ser. **535**, 012005 (2014)
19. C.J. Zhang, J. Xu, Phys. Rev. **C93**(2), 024906 (2016), [1511.03394](#)
20. A. Adare et al. (PHENIX), Phys. Rev. **C85**, 064914 (2012), [1203.2644](#)
21. B.B. Abelev et al. (ALICE), JHEP **06**, 190 (2015), [1405.4632](#)
22. J. Tian, J.H. Chen, Y.G. Ma, X.Z. Cai, F. Jin, G.L. Ma, S. Zhang, C. Zhong, Phys. Rev. **C79**, 067901 (2009), [0906.5287](#)
23. J.C. Dunlop, M.A. Lisa, P. Sorensen, Phys. Rev. **C84**, 044914 (2011), [1107.3078](#)
24. Y. Lu, M. Bleicher, F. Liu, Z. Liu, H. Petersen, P. Sorensen, H. Stoecker, N. Xu, X. Zhu, J. Phys. **G32**, 1121 (2006), [nucl-th/0602009](#)
25. S. Singha, M. Nasim, Phys. Rev. **C93**(3), 034908 (2016), [1603.01220](#)
26. Z.W. Lin, C.M. Ko, B.A. Li, B. Zhang, S. Pal, Phys. Rev. **C72**, 064901 (2005), [nucl-th/0411110](#)
27. X.N. Wang, M. Gyulassy, Phys. Rev. **D44**, 3501 (1991)
28. B. Zhang, Comput. Phys. Commun. **109**, 193 (1998), [nucl-th/9709009](#)
29. Z.W. Lin, Phys. Rev. **C90**(1), 014904 (2014), [1403.6321](#)
30. S.A. Voloshin, A.M. Poskanzer, R. Snellings (2008), [0809.2949](#)
31. J. Xu, C.M. Ko, Phys. Rev. **C83**, 034904 (2011), [1101.2231](#)
32. J. Xu, C.M. Ko, Phys. Rev. **C84**, 014903 (2011), [1103.5187](#)
33. H. Li, L. He, Z.W. Lin, D. Molnar, F. Wang, W. Xie, Phys. Rev. **C93**(5), 051901 (2016), [1601.05390](#)
34. G.L. Ma, Z.W. Lin, Phys. Rev. **C93**(5), 054911 (2016), [1601.08160](#)